J Therm Anal Calorim
DOI 10.1007/s10973-015-4452-0

Ambazone salt with p-aminobenzoic acid

The double benefit of solubility and antibacterial activity improvement

Marieta Mureşan-Pop · Irina Kacsó · Flavia Martin · Simion Simon · Răzvan Ştefan · Ioan Bratu

Received: 13 August 2014 / Accepted: 18 January 2015

Abstract In this study, we obtained a novel salt of ambazone (AMB) with p-aminobenzoic acid (PABA) that exhibits improved solubility and antibacterial activity. The salt was produced by solvent-drop grinding and characterized by powder X-ray diffraction, thermal analysis and Fourier transform infrared spectroscopy. The salt nature of the new form was confirmed by infrared spectroscopy based on the characteristic vibrational band of the protonated amino group. Based on the X-ray powder diffraction data, the compound crystallizes in the triclinic P_{-1} space group with the following unit cell parameters: $a = 14.294$ Å, $b = 9.162$ Å, $c = 8.777$ Å, $\alpha = 95.90°$, $\beta = 100.63°$, $\gamma = 91.73°$. Thermal analysis reveals the thermal events and different decomposition steps of this solid form as compared to the starting compounds. Powder dissolution measurements showed solubility improvement compared with pure ambazone of 2 and 3.3 times in water and phosphate buffer, respectively. Antibacterial tests showed higher activity of the salt to Gram-negative *Escherichia coli* and *Salmonella* bacteria as compared to AMB and PABA. The study demonstrates that the pharmaceutical salt of ambazone with p-aminobenzoic acid (AMB–PABA) can be a possible alternative to ambazone in the treatment of infections with Gram-negative bacteria.

Keywords Salt · Ambazone · p-Aminobenzoic acid · FT-IR · Dissolution · Antibacterial activity

Introduction

Exploring the different solid forms of active pharmaceutical ingredients (APIs) is critical for the successful development of a drug product. Antimicrobial agents are the future in exploring drug resistance of the microbial strains [1]. Obtaining salts or co-crystals of APIs increases the potential of changing and optimizing their physical and chemical properties, such as solubility and bioavailability [2].

Solubility and dissolution rates in aqueous media are important parameters in designing solid dosage forms, as they usually affect the rate of drug absorption and transport in the body. The latest investigations in pharmaceutical industry are focused on the discovery of new salts or co-crystals, the latter providing even higher potential to explore the properties of APIs by using a larger range of pharmaceutically accepted conformers [3, 4].

Ambazone monohydrate (AMB) ([4-(2(Diaminomethylidene)hydrazinyl)phenyl]iminothiourea), $C_8H_{11}N_7S{\cdot}H_2O$, (Fig. 1a) is an antimicrobial agent from the sulfonamides class that possesses antibacterial and antitumor activity [5, 6]. It is active against pathogens and used to treat light throat infections, sometimes replacing the use of antibiotics. The relatively low solubility in water is a significant deficiency of ambazone, which implies the interest of finding new solid forms with improved properties. This compound has a basic character and can exist in different ionized forms of their conjugated acids with pK_a values: 6.22, 7.37 and 10.69 [5].

M. Mureşan-Pop · I. Kacsó (✉) · F. Martin · I. Bratu
National Institute for R&D of Isotopic and Molecular Technologies, 67-103 Donat St., 400293 Cluj-Napoca, Romania
e-mail: iren.kacso@gmail.com

S. Simon
Babes-Bolyai University, 1 Kogalniceanu St., 400084 Cluj-Napoca, Romania

R. Ştefan
Agricultural Sciences and Veterinary Medicine University, 3-5 Calea Manastur St., 400372 Cluj-Napoca, Romania

Published online: 17 February 2015

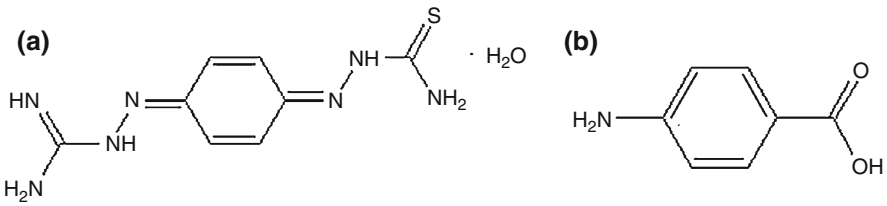

Fig. 1 Structural formula of ambazone monohydrate (**a**) and p-aminobenzoic acid (**b**)

p-Aminobenzoic acid, (PABA) $C_7H_7O_2N$, (Fig. 1b) is a compound of high biological significance with a wide range of therapeutic uses as antioxidant [7], antibacterial [8] or protective drug against UV irradiation [9]. PABA is capable to form extended structures through linear hydrogen bonding associations, through both the carboxylic and amine functional groups [10]. p-Aminobenzoic acid is amphoteric with pK_a's of 2.41 and 4.87 [11].

The interaction between API and a co-former molecule is influenced by ΔpK_a ($\Delta pK_a = pK_a(base) - pK_a(acid)$). The difference between the pK_a values of components is often used to predict whether a salt or co-crystal can be expected for the two components. $\Delta pK_a < 0$ is generally considered to be associated with systems that form co-crystals, $\Delta pK_a > 3$ results in salts, while $0 < \Delta pK_a < 3$ may lead to salt, co-crystal or disordered solid form with partial proton transfer [12–14].

Thermal analysis is commonly used to identify the newly obtained solid forms of pharmaceutical compounds with potential biological activity [1]. Powder X-ray diffraction measurements are carried out to confirm new solid forms of pharmaceuticals and for their structural characterization [15]. FT-IR is a useful technique for the correct identification of solid form nature, salt or co-crystal, based on the characteristic vibrational bands of the protonated amino (NH_3^+) and the carboxylate (COO^-) groups [16, 17].

There are already several salts of ambazone reported with HCl, glutamic acid, niflumic acid and lipoic acid [18–21]. The aim of this study was to obtain a new solid form of AMB with PABA (AMB–PABA), with possibly enhanced solubility and antibacterial activity as compared to AMB.

Materials and methods

Ambazone was provided in monohydrate form by Microsim Laboratories (Romania), and p-aminobenzoic acid was purchased from Sigma-Aldrich. Ultrapure water from Merck was used. All materials were used without prior purification. The AMB–PABA was prepared by solvent-drop grinding (SDG) as follows: an equimolar mixture containing 255.28 mg (1 mmol) of AMB and 137.14 mg (1 mmol) of PABA wetted with few drops of ultrapure water was manually grounded together in an agate mortar for 120 min until a dried powder was obtained.

The obtained powder was analyzed by powder X-ray diffraction, spectroscopic and thermal methods, dissolution and antibacterial studies were also performed.

Powder X-ray diffraction

Powder diffraction patterns were collected in the $2\theta = 3.5$–$43°$ angular domain with a Bruker D8 Advance diffractometer, using Cu $K\alpha_1$ radiation ($\lambda = 1.5406$ Å) (40 kV; 40 mA). In order to increase the resolution, a Ge 111 monochromator was used to eliminate the $K\alpha_2$ radiation. Data collection was performed with the DIFFRAC plus XRD Commander programs' package at room temperature. The step scan mode was performed with a step of 0.01° at a rate of 1 step s^{-1}. The samples were mildly preground in an agate mortar in order to control crystals size and to minimize the preferred orientation effects.

Differential scanning calorimetry

Differential scanning calorimetry (DSC) experiments were performed with a Shimadzu DSC-60 calorimeter, and the sample was heated in the range of 20–300 °C with a heating rate of 10 °C min^{-1} in crimped aluminum sample cell with nitrogen flow of 60 mL min^{-1}. For data collection and analysis, the Shimadzu TA-WS60 and TA60 2.1 software were used.

Differential thermal analysis and thermogravimetry

Simultaneously, differential thermal analysis and thermogravimetry (DTA/TG) measurements were performed with a DTG-60/60H Shimadzu apparatus in the range of 30–400 °C with a heating rate of 10 °C min^{-1}, by using alumina cells (Ø 5.8 mm × 2.5 mm) under dry nitrogen purge (70 mL min^{-1}).

Fourier-transformed infrared spectroscopy

The infrared spectra (FT-IR) were obtained with a JASCO 6100 FT-IR spectrometer using Spectra Manager software

for data collection. Small amount ($\sim$1 mg) of each solid sample (AMB, PABA, AMB–PABA) was mixed with 150 mg of KBr powder and compressed in pellets. The spectra were recorded in the spectral domain 400–4,000 cm^{-1}, with a resolution of 4 cm^{-1} and 256 scans. A KBr pellet was used as reference. Data analysis was performed using Spectra Analysis software.

Powder dissolution experiments

The absorbance values for ambazone and AMB–PABA in different aqueous mediums, deionized water (pH 5.8) and phosphate buffer (pH 7.0), at different times were detected by a μDISS Profiler apparatus. The system consists of an integrated diode array spectrophotometer connected to a fiber optic UV probe located directly in the reaction vessel and is able of measuring the concentration as a function of time without having to filter the solution. The measurement of dissolution kinetics and equilibrium solubility was carried out at 430 nm, where PABA has no absorption and the concentrations of AMB–PABA were calculated by means of a standard curve. The solids of AMB starting material and AMB–PABA were milled to powder and sieved using standard mesh sieves to provide samples with approximate particle size ranges of 150–200 μm. In a typical experiment, 10 mL of aqueous medium was added to a flask containing 1 mg of sample, and the resulting mixture was stirred at 25 °C and 400 rpm.

Antibacterial activity testing

Strains and inoculum preparation: *Escherichia coli* (ATCC-25922), *Salmonella typhimurium (*ATCC-14028*), Staphylococcus aureus* (ATCC-25923) and *Bacillus cereus* (ATCC-10987) bacterial species used in this study were provided by the fermentation laboratory of University of Agricultural Sciences and Veterinary Medicine, Cluj-Napoca. A broth subculture was prepared by inoculating loop full from stock culture of strains into a test tube containing nutrient broth (NB, Merck, Germany), and strains were incubated for 24 h at 37 °C. Incubation for 24 h allowed the bacteria to approach the stationary phase of growth at a concentration of ca. 8 log unit CFU mL^{-1}. The culture was then transferred to 10 mL of fresh and incubated for 24 h at 35 °C to reach a final concentration of 8 log unit CFU mL^{-1}. Growth conditions: the microorganisms were inoculated each one into 25 mL of nutrient broth and incubated overnight at 37 °C with continuous agitation in an Orbital Shaker (Heidolph Unimax 1100 coupled with incubator Heidolph Unimax 1000). The agitation speed was set at 200 rpm. Each of these overnight cultures was used to inoculate 25 mL volumes of nutrient broth (in triplicate) to a standardized optical density of between 0.005 and 0.010 at a wavelength of 600 nm (OD600). Growth values were obtained by measuring the turbidity at OD600 by Nanodrop ND-1000 Spectrophotometer UV–Vis (Nanodrop Technologies USA) of the test strains over a period of 48 h. After 48 h, viable counts were determined by serial dilution of the broth into 0.1 % peptone water and plating on to nutrient agar plates (Oxoid). All plates were incubated overnight in air at 37 °C for 24–48 h, and the resulting colonies were counted. In parallel, each 'glass powder' of 43.75 mg was added to specify growth agar (Levine for *E.coli* and Oxford for *L. monocytogenes*) with 50 μL of inoculum and incubated overnight in air at 35 °C for 24–48 h, the resulting colonies were counted.

Results and discussion

ΔpKa calculation

The pKa values for AMB are 10.69 for equilibrium between the negatively charged and neutral forms, 7.39 for equilibrium between the neutral and single positively charged and 6.22 for equilibrium between the singly and double positively charged forms [5]. In the case of PABA, the pKas of the amino and carboxyl groups are 2.41 and 4.87, respectively [11]. The ΔpKa between the two neutral forms of base and acid is 5.84. Since the value is >3, according to the ΔpKa rule, it is expected to form a salt.

Powder X-ray diffraction analysis

The powder X-ray diffraction patterns of the AMB, PABA and AMB–PABA compounds are shown in Fig. 2.

One can see that the powder diffraction pattern of AMB–PABA solid form is different from the XRPD patterns of both AMB and PABA. In order to evaluate whether AMB–PABA is a single phase or a mixture of phases, we attempted to index the X-ray powder pattern and to determine the unit cell parameters using X-Cell method [22].

The AMB–PABA compound crystallizes in the triclinic system with the following unit cell parameters: $a = 14.294$ Å, $b = 9.162$ Å, $c = 8.777$ Å, $\alpha = 95.90°$, $\beta = 100.63°$, $\gamma = 91.73°$. Assuming two AMB–PABA molecules in the unit cell, the calculated density is $\rho = 1.66$ g cm^{-3}, which is in agreement with the triclinic P_{-1} space group. The results of the indexing procedure indicated that AMB–PABA is a single form.

In order to characterize the crystallinity of the new compound, the crystallite size was evaluated using Scherrer equation [23] ($D_{hkl} = 0.89\,\lambda/(\beta_{hkl}\cdot\cos\theta)$), where β_{hkl} is the FWHM (Full Width at Half Maximum) of the diffraction peaks corrected for the contributions due to the diffractometer.

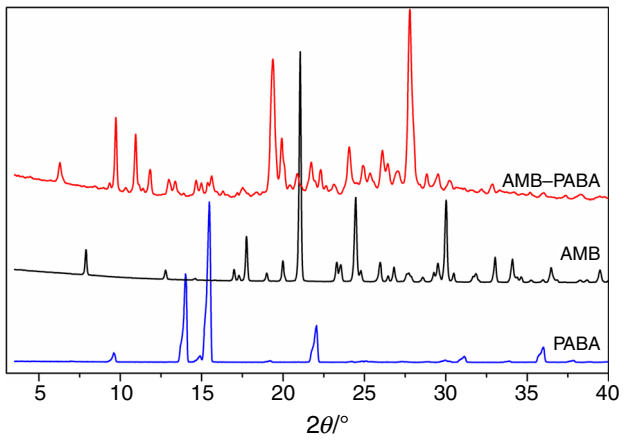

Fig. 2 Experimental powder X-ray diffraction patterns of AMB, PABA and AMB–PABA

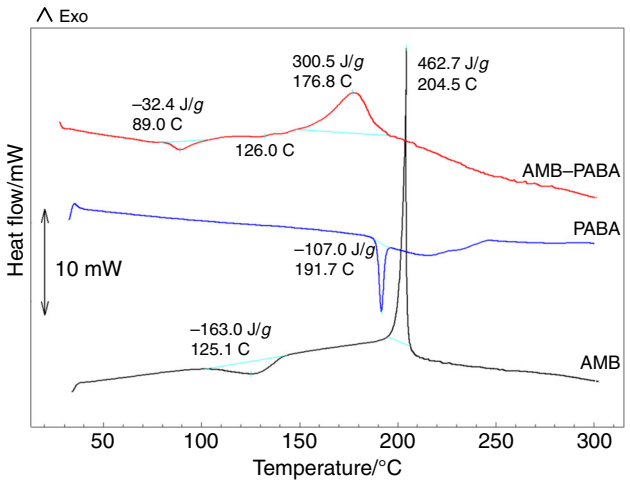

Fig. 3 DSC curves of AMB, PABA and AMB–PABA

The following crystallite sizes were obtained: 480 Å for AMB–PABA and 1,360 Å for AMB; it can be noticed that crystallite size of the compound obtained by SDG method is smaller.

Additionally, the amorphous content of AMB and AMB–PABA powders was estimated by using the background subtraction method implemented in Material Studio software (Materials Studio, release 5.5., Accelrys Software Inc., San Diego, CA, USA, http://accelrys.com/products/materials-studio/). This method provides a rough estimation of the crystallinity and does not require reference XRPD patterns of the pure crystalline or amorphous phases. We obtained 93 % crystallinity for AMB, and the crystallinity of AMB–PABA decreased to 70 %, probably due to the fact that it was obtained by the grinding method, which is usually generating some amorphous content.

Thermal analysis

The DSC curves of AMB, PABA and of AMB–PABA are presented in Fig. 3. For AMB, a broad endothermic peak between 107 and 140 °C can be identified with a maximum at 125.1 °C and heat of dehydration of −163 J g^{-1}. This peak corresponds to the loss of the bounded water molecules. Another sharp exothermic peak appears between 201 and 205 °C with a maximum at 204.5 °C and 462.7 J g^{-1} heat of process, due to the melting with decomposition of AMB [20, 21]. The DSC curve of PABA presents a sharp endothermic peak between 189 and 194 °C with maximum at 191.7 °C and heat of fusion of −107 J g^{-1} [24, 25], corresponding to the melting process followed by the degradation of the substance.

The DSC curve of AMB–PABA presents three thermal events: an endothermic peak between 83 and 95 °C with peak maximum at 89 °C and −32.4 J g^{-1} heat of dehydration corresponding to the loss of non-bounded water molecules. This event is followed by a solid–solid transformation at 126 °C and a broad exothermic peak between 161 and 186 °C with peak maximum at 176.8 °C and heat of process of 300.5 J g^{-1}, probably due to the melting with decomposition of the amorphous sample.

The simultaneously DTA/TG analyses for AMB were already reported by us [19–21]. TG curve of AMB shows first mass loss of 6.6 %, corresponding to the release of water, in good agreement with the theoretical water content (7 %) of the ambazone monohydrate. Other two mass losses of 27.4 % and 8.6 % between 190 and 400 °C correspond to AMB decomposition.

For AMB–PABA sample (Fig. 4), the water loss occurs at a lower temperature than for pure AMB, in two steps corresponding to large endothermic peaks in the DTA curve: between 50 and 83 °C with maximum at 63.5 °C and between 84 and 115 °C with maximum at 91.5 °C associated with two mass losses of 5.2 and 4.2 %, respectively.

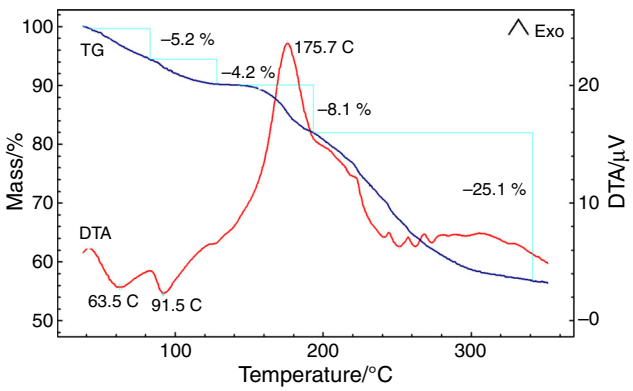

Fig. 4 TG/DTA curves of AMB–PABA

A mass loss of 8.1 % occurs in the 140–193 °C temperature range, which corresponds to a broad exothermic peak with maximum at 175.7 °C, indicating the start of degradation. The last 25.1 % mass loss is the most significant, and occurs in the temperature range 193–350 °C, corresponding to the elimination of volatile components resulting from compound decomposition.

For AMB–PABA sample (Fig. 4), the first two mass losses of 5.2 and 4.2 %, respectively, occur at a lower temperature than for pure AMB and correspond to the large endothermic peaks in the DTA curve: between 50 and 83 °C with maximum at 63.5 °C and between 84 and 115 °C with maximum at 91.5 °C. The first 5.2 % mass loss in the lower temperature range is likely related to non-bounded water molecule that is easily released from the solid material. The 4.2 % mass loss in the higher temperature range could be embedded in the crystal structure, leading to a monohydrated salt form (theoretical mass loss corresponding to one water molecule is 4.6 %).

Decomposition processes of AMB–PABA occur in the temperature intervals of 140–193 and 193–350 °C with mass losses of 8.1 and 25.1 %, respectively.

The DTA/TG data are in good agreement with the DSC results and show a different thermal behavior of the AMB–PABA versus AMB and PABA starting materials.

Spectroscopic analysis

Based on FT-IR analysis of a carboxylic acid and an organic base system, the C=O stretching frequencies are a preliminary indication whether the complex is a co-crystal or a salt. The stretching band of carboxylic acid, bonded to an aromatic ring, appears at around 1,700 cm^{-1}, while the carboxylate ion displays a strong asymmetrical stretching band around 1,650–1,550 cm^{-1} and a weaker symmetric stretch ~1,400 cm^{-1}. The asymmetric bending vibrations of protonated amino group NH_3^+ are located around 1,640–1,570 cm^{-1} [16, 17]. It is difficult to assign carbonyl stretch and NH bend frequency reliably because they appear close to each other.

FT-IR absorption spectra of AMB, PABA and AMB–PABA are presented in Fig. 5a, b. In the 3,400–3,200 cm^{-1} spectral range (Fig. 5a), the NH stretching vibrations of pure AMB can be assigned to primary amines at ~3,399, 3,324 and ~3,231 cm^{-1} [17–19, 26–28]. These bands were shifted by 12–16 cm^{-1} to ~3,387 and 3,247 cm^{-1}, respectively, in AMB–PABA spectrum. The band located at ~3,147 cm^{-1} corresponds to the secondary amine stretching vibration of AMB [18, 28] and is shifted with 10 cm^{-1} to 3,157 cm^{-1} in the AMB–PABA spectrum.

In the IR spectrum of PABA, the vibrations of the N–H bonds in the primary amino group are registered with maxima at 3,466, 3,362 and 3,231 cm^{-1}, respectively [29].

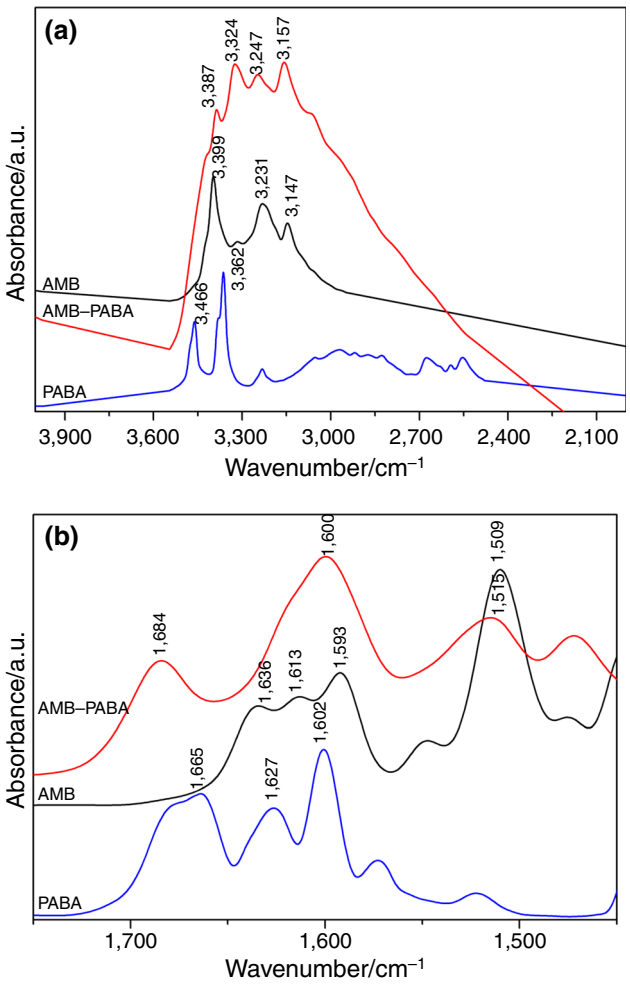

Fig. 5 FT-IR spectra of AMB, PABA and AMB–PABA in **a** 4,000–2,000 cm^{-1}, **b** 1,750–1,450 cm^{-1} spectral domain

In the 1,750–1,450 cm^{-1} spectral domain of AMB spectrum (Fig. 5b), the band at 1,593 cm^{-1} is assigned to C=N asymmetric stretching vibration, the band at 1,613 cm^{-1} is attributed to the primary amine and the deformation region of secondary amino group is located at 1,509 cm^{-1} [18, 28, 29]. The secondary amine vibration at 1,509 cm^{-1} is shifted to 1,515 cm^{-1} in the AMB–PABA spectrum, similarly as in the AMB–HCl system [18].

The stretching vibration of the C=O bond in the carboxyl group of PABA is observed at 1,665 cm^{-1}. The absorption bands with maxima at 1,627 and 1,602 cm^{-1} belong to the deformation vibrations of the N–H bonds in the amino group and to valence vibrations of the C=C bonds in the benzene ring, respectively [30].

In the AMB–PABA spectrum, a new strong absorption band appears at 1,684 cm^{-1}, which is assigned to deformation vibration of the protonated amino group [31].

The band at 1,613 cm^{-1} (NH_2) of AMB and the band at 1,665 cm^{-1} (C=O) of PABA shifted and then merged under a strong broad band between 1,650 and 1,550 cm^{-1}

which covers the N–H bending vibration of protonated amino group of AMB and the C=O asymmetrical stretching band of carboxylate group of PABA, respectively. The weaker band at 1,424 cm^{-1} is assigned to symmetric stretching of the carboxylate ion [16, 32]. The observed changes in the absorption bands of the amino and carboxyl groups can be attributed to an ionic interaction between the carboxyl group of PABA and the amino group of AMB, confirming the salt nature of the AMB–PABA form.

Dissolution testing results

Dissolution profiles of pure AMB and AMB–PABA salt, in deionized water (pH 5.8) and in phosphate buffer (pH 7.0), are shown in Fig. 6a, b. In our experiments, the solubility value of AMB monohydrate in water was higher than that reported by Löber and Hoffman (0.02 mg mL^{-1}) [5].

For the AMB–PABA salt, the powder dissolution measurements revealed a faster dissolution rate in deionized water and the solubility was found to be approximately two times larger than in the case of AMB.

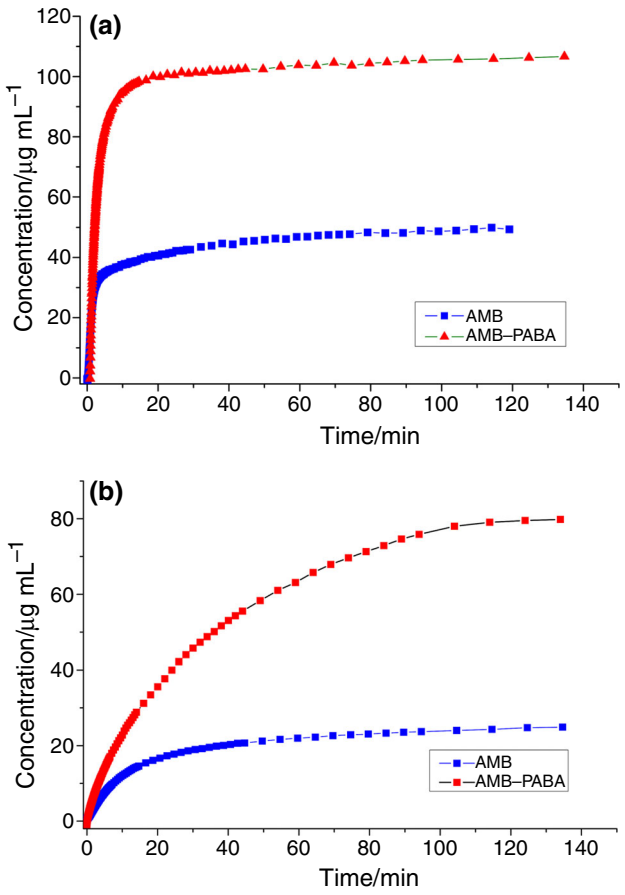

Fig. 6 Dissolution profiles for AMB and AMB–PABA in **a** deionized water, **b** phosphate buffer

The dissolution experiments in phosphate buffer showed that AMB has a lower solubility than in deionized water, but the solubility of the AMB–PABA was improved by 3.3 times compared with pure AMB.

After the dissolution experiments, the undissolved solid was filtered and air-dried and the solid form stability of AMB–PABA was confirmed by XRPD analyses.

Antibacterial testing

The investigated compounds AMB, PABA and AMB–PABA were evaluated for their antibacterial activity against two Gram-negative bacteria (*E. coli* and *S. typhimurium*) and Gram-positive bacteria (*S. aureus* and *B. cereus*). In all investigated strain cultures, all compounds exhibit antibacterial effect as illustrated in Fig. 7 where the comparative action is given. The Gram-positive bacteria, *S. aureus* and *B. cereus*, are more sensitive to the interaction with the compounds.

The optical densities of the control samples for both strains, being pure cultures, are similar: 0.056 for the first and 0.051 for the last one. The optical densities for the broth impurities with compounds lie between 0.004 and 0.006 for *S. aureus* and between 0.004 and 0.009 for *B. cereus,* respectively, and demonstrate their higher antibacterial effect.

For the Gram-negative bacterial strains, the effect is dramatically different for the starting compounds and for the ending one. Thus, both AMB and PABA show similar effect upon *E. coli*, and the optical densities for the mixtures are 0.061 and 0.056, respectively. *Salmonella* is more sensitive to the action AMB and PABA, the optical density being 0.035 and 0.027, respectively, much lower than for *E. coli.* Both inhibit the bacterial growth when compared to the control variant whose optical density is about 0.08.

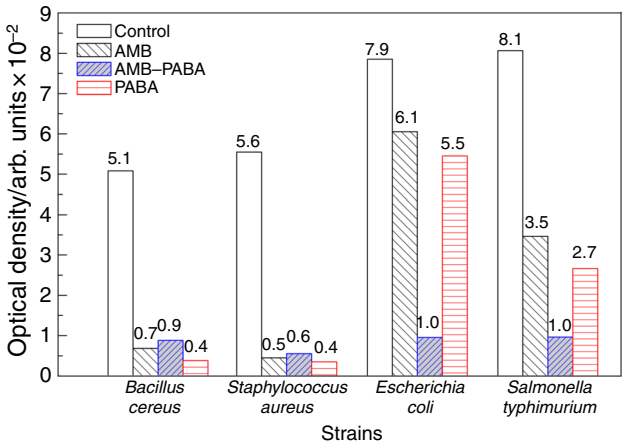

Fig. 7 Antibacterial effects of control, AMB, PABA and AMB–PABA on Gram-positive and Gram-negative bacteria

At the same time, the action of the crystallized sample AMB–PABA is much more intense than the starting powder ones for both Gram-negative strains, its optical density being 0.01.

Conclusions

We have presented here the novel salt of ambazone with p-aminobenzoic acid obtained by water-drop grinding. Indexing of the X-ray powder diffraction pattern showed that AMB–PABA is a single form and it crystallizes in the P_{-1} triclinic system. The thermal behavior described by DSC and TG/DTA traces showed significant differences between the thermal events and the decomposition steps of the novel salt form and the starting compounds. The FT-IR analysis confirmed the salt formation by changes in the characteristic absorption bands of the amino and carboxyl groups with the appearance of the vibrations of protonated amino group of AMB and the carboxylate group of PABA, respectively, attributed to an ionic interaction.

The AMB–PABA solid form was stable and showed substantial solubility improvement compared with ambazone in deionized water and phosphate buffer (pH 7.0). Additionally, antibacterial activity of AMB–PABA to Gram-negative bacteria was synergistically improved compared with single AMB and PABA compounds.

The results show the potential of the AMB–PABA salt form to be developed in an oral formulation with improved solubility and bioavailability compared with the poorly water-soluble ambazone. Moreover, the enhanced antibacterial activity demonstrates that the pharmaceutical salt of ambazone with p-aminobenzoic acid (AMB–PABA) can be a possible alternative to ambazone in the treatment of infections with Gram-negative bacteria.

Acknowledgements Authors are grateful for antibacterial studies performed by Dr. Dan Vodnar from USAMV, Cluj-Napoca and Sorina Ciupe, for FT-IR measurements. This work was supported by POS CCE–A2 O2.1.2, PN 09-44 02 01 and PN 09-44 02 05 projects.

References

1. Hollo B, Rodic MV, Vojinovic-Jesic LS, Zivkovic-Radovanovic V, Vucković G, Leovac VM, Mészáros Szécsényi K. Crystal structure, thermal behavior, and microbiological activity of a thiosemicarbazide-type ligand and its cobalt complexes. J Therm Anal Calorim. 2013. doi:10.1007/s10973-013-3489-1.
2. Brittain HG. Polymorphism in pharmaceutical solids, vol. 192. 2nd ed. New York: Informa Healthcare; 2009.
3. Lu J. Crystallization and transformation of pharmaceutical solid forms. Afr J Pharm Pharmacol. 2012;6:581–91.
4. Braga D, Grepioni F, Maini L, Polito M. Crystal polymorphism and multiple crystal forms. Struct Bond. 2009;132:25–50.
5. Löber G, Hoffmann H. Ambazone as a membrane active antitumor drug. Biophys Chem. 1990;35:287–300.
6. Kühnel HJ, Amlacher R, Baumgart J, Schulze W. Distribution of 14C-ambazone in normal and leukemia P 388-bearing mice. Arch Geschwulstforsch. 1988;58:217–22.
7. Akberova SI. New biological properties of p-aminobenzoic acid. Biol Bull. 2002;29:390–3.
8. Richards RME, Xing DKL. The effect of p-aminobenzoic acid on the uptake of thymidine and uracil by *Escherichia coli*. Int J Pharm. 1995;116:217–21.
9. Xavier S, Macdonald S, Roth J, Caunt M, Akalu A, Morais D, Buckley MT, Liebes L, Formenti SC, Brooks PC. The vitamin-like dietary supplement para-aminobenzoic acid enhances the antitumor activity of ionizing radiation. Int J Radiat Oncol Biol Phys. 2006;65:517–27.
10. Crisan ME, Bourosh P, Maffei ME, Forni A, Pieraccini S, Sironi M, Chumakov YM. Synthesis, crystal structure and biological activity of 2-hydroxyethylammonium salt of p-aminobenzoic acid. PLoS ONE. 2014;9:e101892.
11. Lukfics M, Barcsa G, Kovfics-Hadady K. The effects of pH, ionic strength and buffer concentration of mobile phase on R_F of acidic compounds in ion-pair TLC. Chromatographia. 1998;48:511–6.
12. Stevens JS, Byard SJ, Schroeder SLM. Characterization of proton transfer in co-crystals by X-ray photoelectron spectroscopy (XPS). Cryst Growth Des. 2010;10:1435–42.
13. Childs SL, Stahly GP, Park A. The salt-cocrystal continuum: the influence of crystal structure on ionization state. Mol Pharm. 2007;4:323–38.
14. Stahl PH, Wermuth CG. Handbook of pharmaceutical salts: properties, selection, and use. 2nd rev ed. Weinheim: Wiley-VCH; 2011.
15. Tjahjono M, Schreyer MK, Guo L, Garland M. Determination of the individual specific heat capacities of solids from multi-component powder mixtures and polymorphic mixtures. J Therm Anal Calorim. 2012;108:361–70.
16. Sarma B, Chen J, Hsi HY, Myerson AS. Solid forms of pharmaceuticals: polymorphs, salts and cocrystals. Korean J Chem Eng. 2011;28:315–22.
17. Ivanova B, Spiteller M. Salts of aromatic amines: crystal structures, spectroscopic and non-linear optical properties. Spectrochim Acta A. 2010;77:849–55.
18. Mureşan-Pop M, Kacsó I, Tripon C, Moldovan Z, Borodi G, Bratu I, Simon S. Spectroscopic and structural study of the ambazone hydrochloride. J Therm Anal Calorim. 2011;104:299–306.
19. Mureşan-Pop M, Kacsó I, Filip X, Vanea E, Borodi G, Leopold N, Bratu I, Simon S. Spectroscopic and physical–chemical characterization of ambazone–glutamate salt. Spectroscopy. 2011;26:115–28.
20. Kacsó I, Rus L, Pop M, Borodi G, Bratu I. Structural characterization of ambazone salt with niflumic acid. Spectroscopy. 2012;27:49–58.
21. Kacsó I, Racz C, Santa S, Rus L, Dadarlat D, Borodi G, Bratu I. Ambazone lipoic acid salt: structural and thermal characterization. Thermochim Acta. 2012;550:13–8.
22. Neumann MA. X-Cell: a novel indexing algorithm for routine tasks and difficult cases. J Appl Crystallogr. 2003;36:356–65.
23. Britto S, Joseph S, Kamath PV. Distinguishing crystallite size effects from those of structural disorder on the powder X-ray diffraction patterns of layered materials. J Chem Sci. 2010;122:751–6.
24. Kacso I, Borodi G, Farcas SI, Hernanz A, Bratu I. Host–guest system of Vitamin B10 in β-cyclodextrin: characterization of the interaction in solution and in solid state. J Incl Phenom Macrocycl Chem. 2010;68:175–82.
25. Rotich MK, Glass BD, Brown ME. Thermal studies on some substituted aminobenzoic acids. J Therm Anal Calorim. 2001;64:681–8.
26. Bugay DE, Brittain HG. Infrared absorption spectroscopy. In: Brittain HG, editor. Spectroscopy of pharmaceutical solids. New York: Informa Healthcare; 2006.

27. Koleva BB, Kolev T, Seidel RW, Spiteller M, Mayer-Figge H, Sheldrick WS. Self-assembly of hydrogensquarates: crystal structures and properties. J Phys Chem A. 2009;113:3088–95.
28. Socrates G. Infrared and Raman characteristic group frequencies: tables and charts. 3rd ed. Chichester: Wiley; 2001.
29. Roik NV, Belyakova LA. IR spectroscopy, X-Ray diffraction and thermal analysis studies of solid "b-Cyclodextrin–Para-Aminobenzoic Acid" inclusion complex. Phys Chem Solid State. 2011;12:168–73.
30. Robinson RA, Biggs AI. The ionization constants of p-aminobenzoic acid in aqueous solutions at 25c. Aust J Chem. 1956;10:128–34.
31. Cleaves AP, Plyler EK. The infra-red absorption spectrum of methylamine vapor. J Chem Phys. 1939;7:563–9.
32. Sarmento B, Ferreira D, Veiga F, Ribeiro A. Characterization of insulin-loaded alginate nanoparticles produced by ionotropic pregelation through DSC and FTIR studies. Carbohydr Polym. 2006;66:1–7.